

## Supporting Information

### **Se-induced heterostructure electrode with polymetallic-CoNiFe towards high performance supercapacitors**

Liyun Zhao<sup>a</sup>, Haoran Guo<sup>a</sup>, Yanyan Li<sup>a</sup>, Zhengyuan Liu<sup>a, b</sup> Rui Song<sup>a\*</sup>

<sup>a</sup>School of Chemical Sciences, University of Chinese Academy of Sciences, 19 Yuquan Road, Shijingshan District, Beijing, 100049, P R China

<sup>b</sup>Sino-Danish College, University of Chinese Academy of Sciences (UCAS), P R China

\*Email: [rsong@ucas.ac.cn](mailto:rsong@ucas.ac.cn)

## Experimental section

**Pre-treatment of carbon fiber cloth (CC):** First, several pieces of CC (2 cm×3 cm) were immersed in 6 M HNO<sub>3</sub> solution at 80°C overnight to eliminate surface oxides. After that, the carbon fiber cloth was subjected to 30 minutes of ultrasonic cleaning and rinsing with deionized water, followed by drying for later use.

**Synthesis of other contrast electrodes:** For comparison, a precursor containing only one metal salt (Co/Ni/Fe) was also synthesized under the same conditions (Co-pre, Ni-pre, Fe-pre). Similarly, the above comparison samples are also prepared under the same selenization conditions (Co-Se, Ni-Se, Fe-Se).

**Assembly of flexible all-solid Hybrid Asymmetric Supercapacitors:** To prepare the gel electrolyte for ASC, 3 g of polyvinyl alcohol (PVA) and 2 g of potassium hydroxide (KOH) are added to 36 mL deionized water. The resulting solution is heated to 90°C until a gel is obtained. The positive electrode material (CoNiFe-Se, 1×1 cm<sup>2</sup>) and negative electrode material (AC electrode prepared using slurry coating technique, with AC powder, conductive carbon black, and polyvinylidene fluoride (PVDF) added in an 8:1:1 ratio, and the slurry prepared using N-methyl-2-pyrrolidone (NMP) solvent, then coated on a conductive carbon fiber cloth to form a 1×1 cm<sup>2</sup> electrode) are immersed in the PVA/KOH electrolyte for 1 minute, after which the electrodes are immersed repeatedly. The electrodes are then dried for 12 hours before being assembled into flexible all-solid-state (ASC) CoNiFe-Se//AC.

## Characterization methods

The crystal structure was analyzed by X-ray diffractometry (XRD, Smartlab, Cu K $\alpha$ ) in the range of 10-60°. In addition, a Renishaw Invia Raman spectrometer with a 532 nm, 20 mW Ar<sup>+</sup> laser source was used to collect Raman spectra. Scanning electron microscopy (SEM) was carried out on a Hitachi SU8220 to study morphology and structure of the sample. Transmission electron microscopy (TEM, Tecnai F20, STWIN) in conjunction with energy-dispersive X-ray spectroscopy (EDS) is also performed to detect the microstructure of the active material. X-ray photoelectron spectroscopy (XPS) is measured on a Thermo Scientific ECSALab 250Xi X-ray photoelectron

spectrometer using Al K $\alpha$  radiation (1486 eV) to study the chemical state and surface composition. Electron paramagnetic resonance (EPR) is measured by an A300-10/12 of Bruker, Germany. Raman spectra were examined using a Renishaw Invia Raman spectrometer with a 532 nm laser source. The static-water-droplet angles and air-bubble contact angles measurements were performed via a Dataphysics-OCA100, Germany.

### **Electrochemical measurements**

**Evaluation of Supercapacitive Performances:** All electrochemical measurements are based on the CHI 660E electrochemical workstation (CH Instrumental Co., Ltd, Shanghai) using a three-electrode electrochemical cell (graphite rod as the counter electrode, a saturated calomel electrode (SCE) as the reference electrode, and a self-supported CoNiFe-Se single electrode as the working electrode). In this system, a 6M KOH aqueous solution is used as the electrolyte, and the stability of the electrode is tested at a scan rate of 10 mV s<sup>-1</sup>. In addition, the frequency range of electrochemical impedance spectroscopy (EIS) measurements is from 0.01Hz to 100KHz. Constant current charge-discharge (GCD) testing is also conducted in the range of -0.1V to 0.45V, and the specific capacitance ( $C_s$ ) is calculated using the following equation:

$$C_s = It/A\Delta V \quad (1)$$

Where  $C_s$  is the areal specific capacitance (mF cm<sup>-2</sup>),  $I$  is the discharge current (A),  $t$  is the discharge time (s),  $A$  represents the area of self-supported electrodes (cm<sup>2</sup>) and  $\Delta V$  is the potential window (V).

In addition, the energy density and power density of ASC are calculated using the following two equations:

$$E = 1/2 C_s V^2 \quad (2)$$

$$P = E/t \quad (3)$$

Where  $E$  represents the energy density ( $\mu$  Wh cm<sup>-2</sup>),  $C_s$  is the areal specific capacitance (F cm<sup>-2</sup>),  $V$  means the operating voltage (V),  $P$  is the power energy ( $\mu$  W cm<sup>-2</sup>),  $t$  refers to the discharge time (s).

Also, to achieve  $q^+=q^-$ , the mass ratio of the positive electrode active material to the negative electrode active material is determined by the following equation:

$$m_+ : m_- = \left( \int \frac{idV}{v} \right) - : \left( \int \frac{idV}{v} \right) + \quad (4)$$

The mass ratio of the positive electrode active material to the negative electrode active materials was determined from the cyclic voltammetry acquired at 10mV s<sup>-1</sup> for both electrodes.

### **DFT calculation**

First-principles calculations were performed within the density functional theory framework.<sup>1</sup> The projector-augmented wave (PAW) method and the generalized gradient approximation (GGA) for the exchange-correlation energy functional, as implemented in the Vienna ab initio simulation package (VASP) were used.<sup>2-4</sup> The GGA calculation was performed with the Perdew-Burke-Ernzerhof (PBE) exchange-correlation potential.<sup>5</sup> Considered long-range interaction between molecules/intermediates and surface, Van der Waals interactions were considered using DFT-D3 correlation.<sup>6</sup> The convergence criterion of geometry relaxation was set to 0.03 eV·Å<sup>-1</sup> in force on each atom. The energy cutoff for plane wave-basis was set to 600 eV. The K points were sampled with 13×3×4 and 2×2×1 by Monkhorst-Pack method for pristine (CoNiFe)<sub>2</sub>(OH)<sub>2</sub>CO<sub>3</sub> unitcell and CoSe<sub>2</sub>/NiFe<sub>2</sub>O<sub>4</sub> heterostructure, respectively.<sup>6-11</sup>

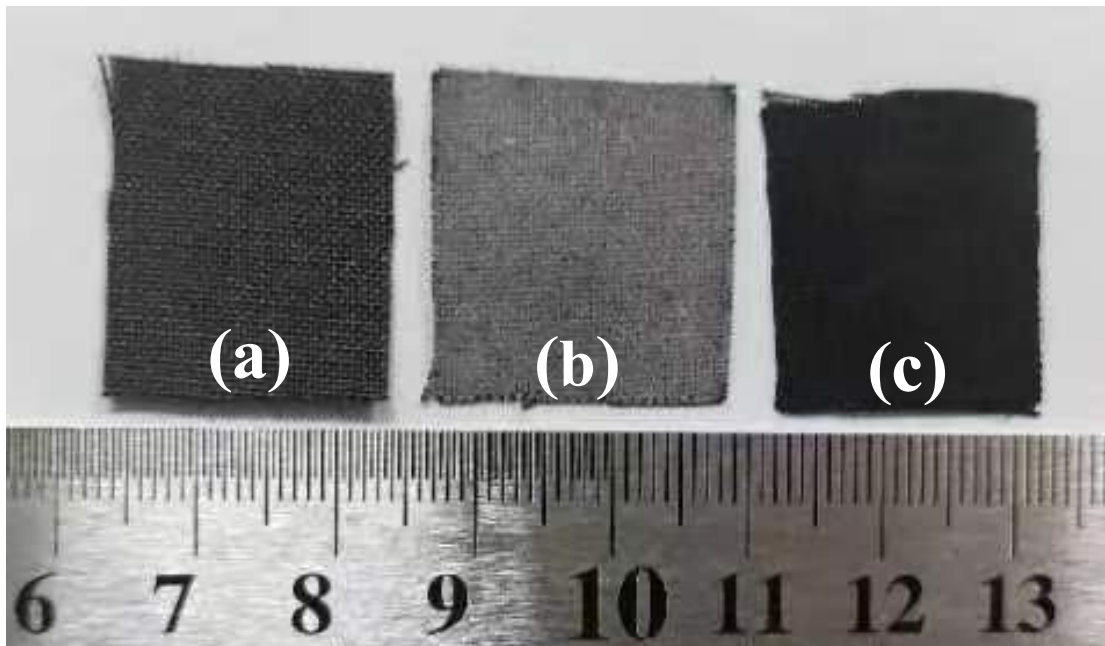


**Figure S1.** Photographs of (a) CC, (b) CoNiFe-pre, (c) CoNiFe-Se.

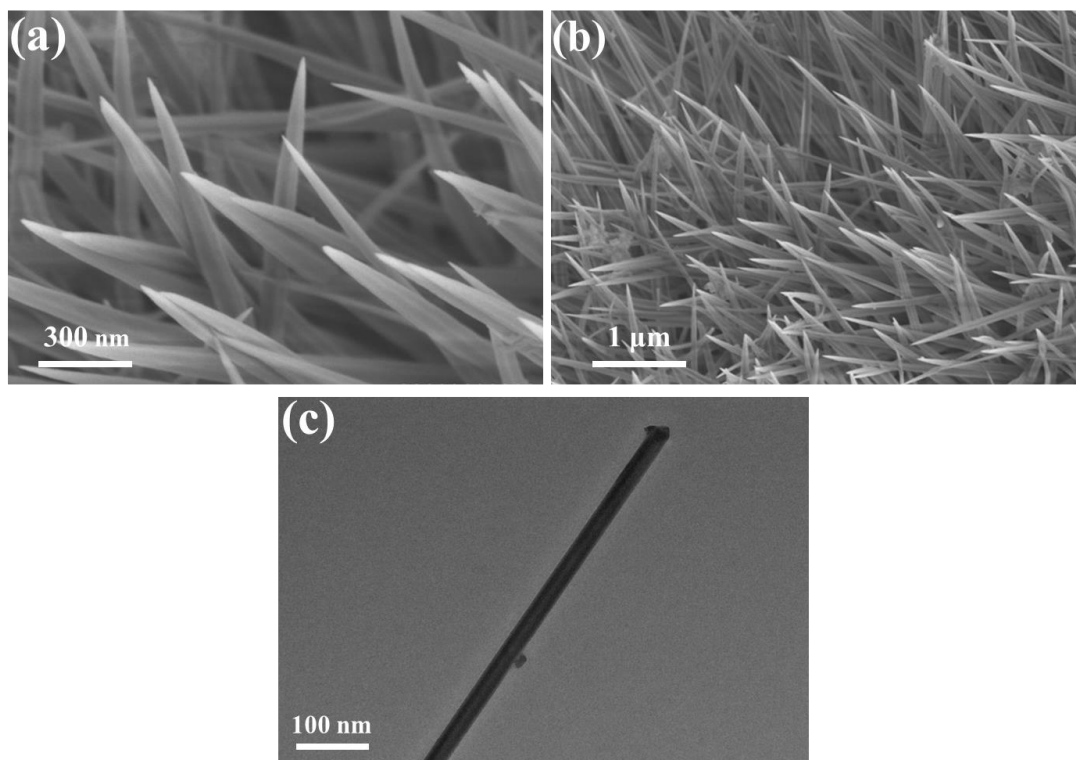


**Figure S2.** (a, b) SEM, (c) TEM images of CoNiFe-pre.

CoNiFe-pre nanoneedles with an average diameter of 130 nm and a smooth surface are uniformly and densely arranged on CC. The vertical orientation of CoNiFe-pre nanoneedles provides favorable conditions for the subsequent growth of heterojunctions. It can also be inferred from TEM that CoNiFe-pre nanoneedles exhibit uniform density and smooth surface.

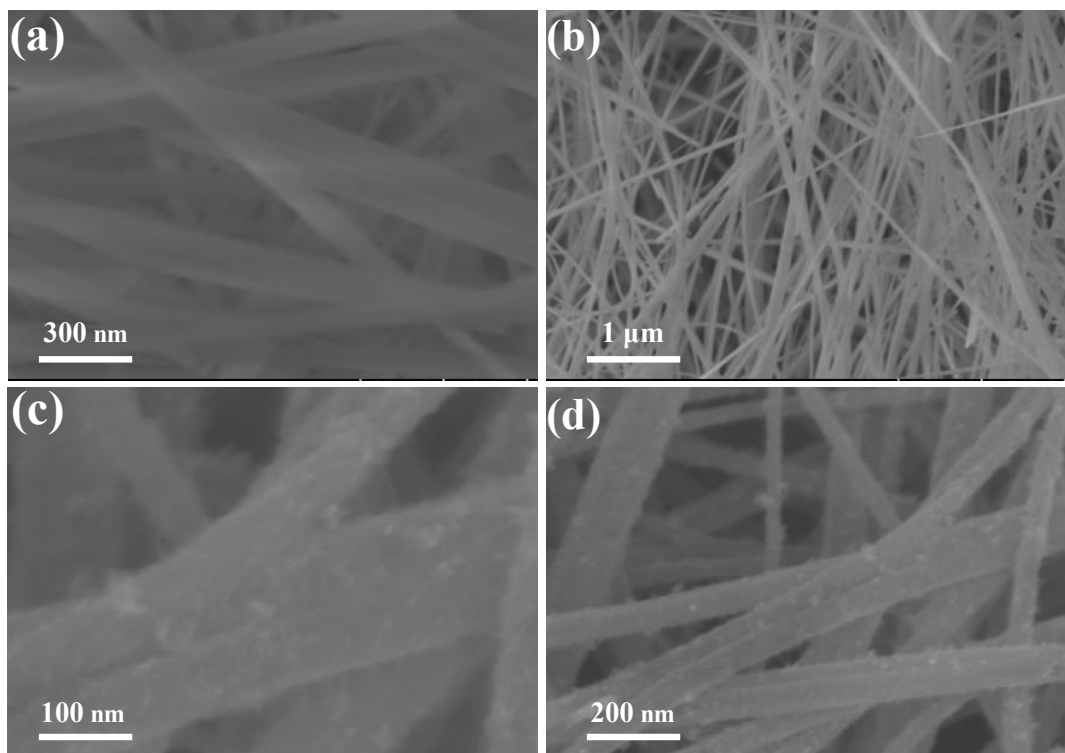


**Figure S3.** SEM images of (a, b) Co-pre, (c, d) Co-Se.

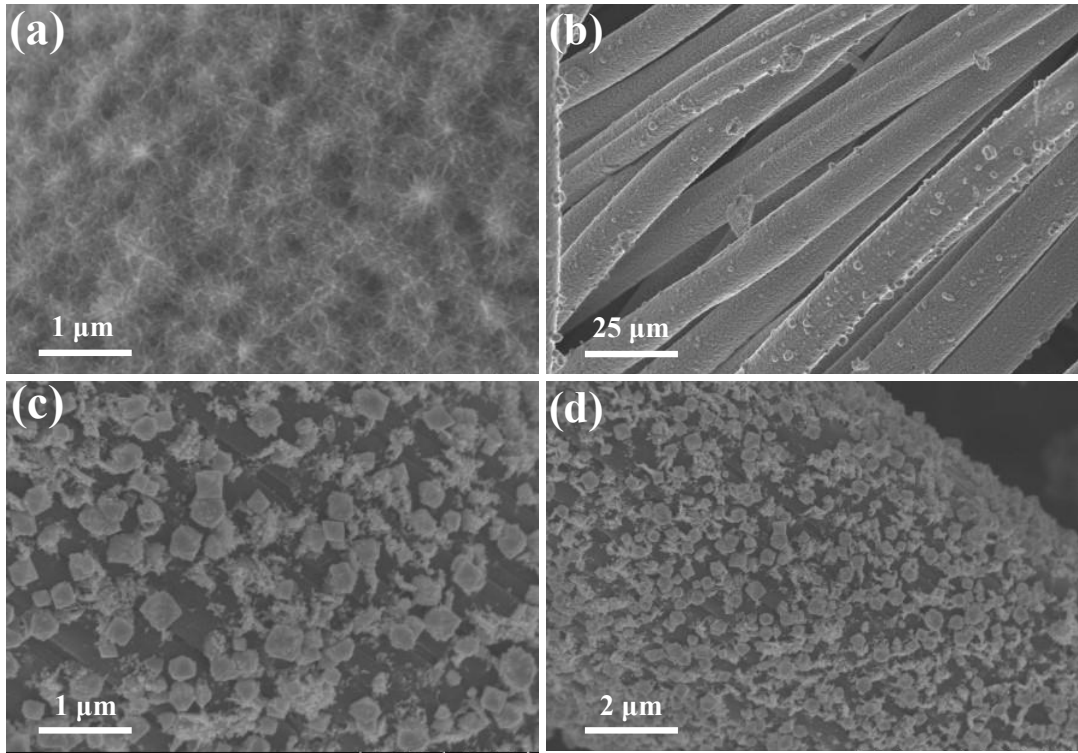


**Figure S4.** SEM images of (a, b) Ni-pre, (c, d) Ni-Se.

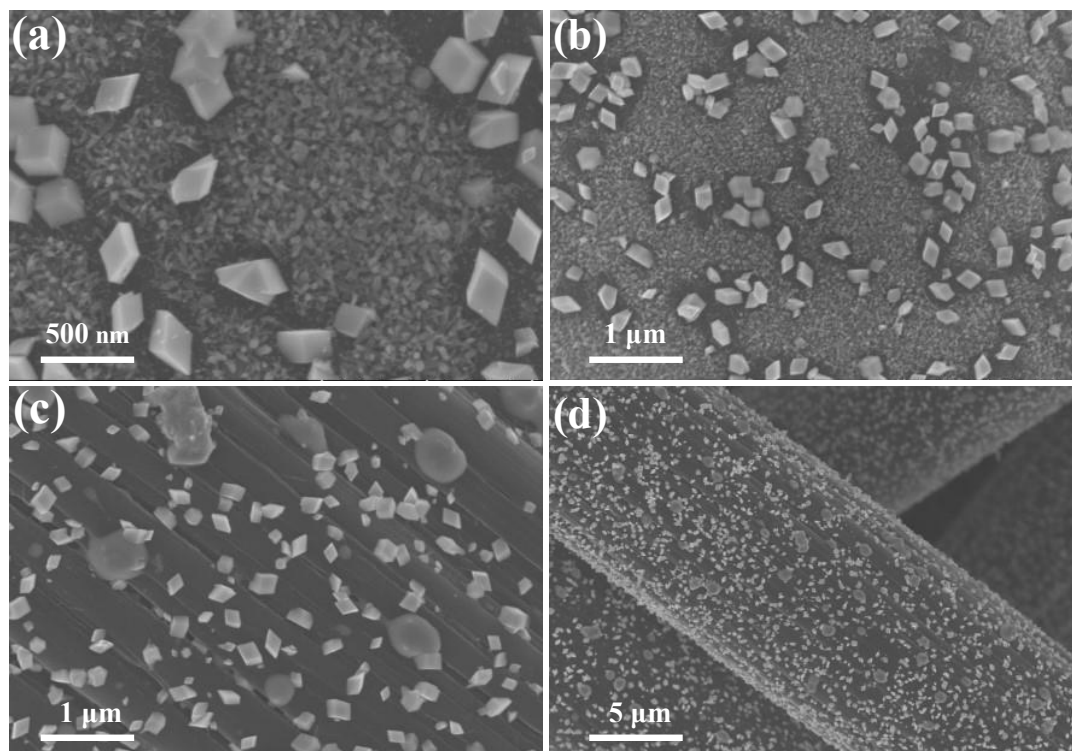


**Figure S5.** SEM images of (a, b) Fe-pre, (c, d) Fe-Se.

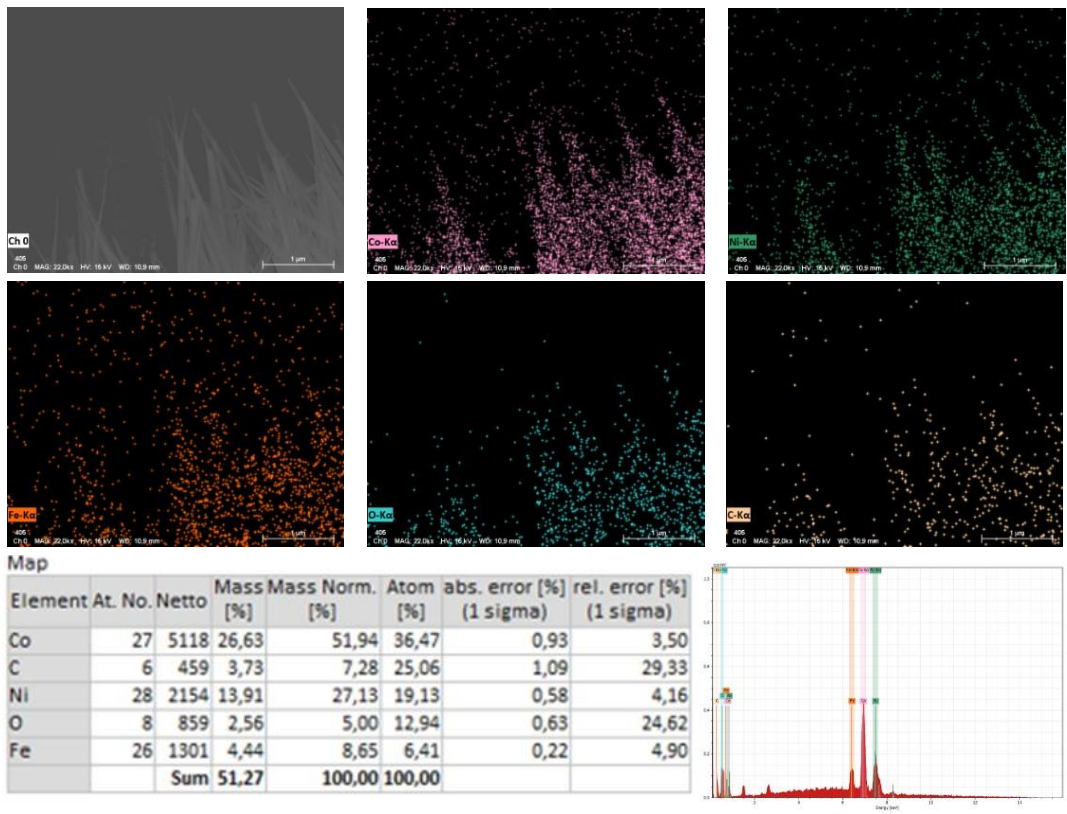
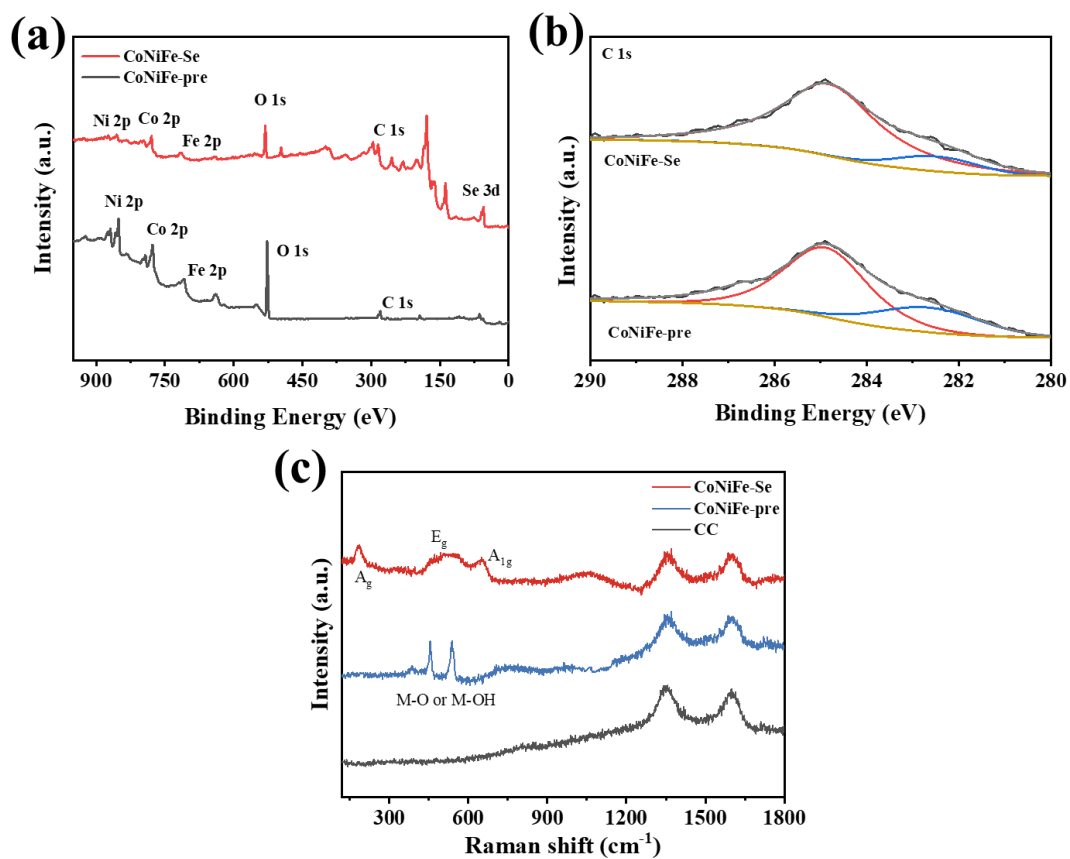


Figure S6. The EDS analyses of CoNiFe-pre.



**Figure S7.** (a) Full scale survey XPS spectrum, (b) C 1s spectra, (c) Raman spectra of CoNiFe-pre and CoNiFe-Se.

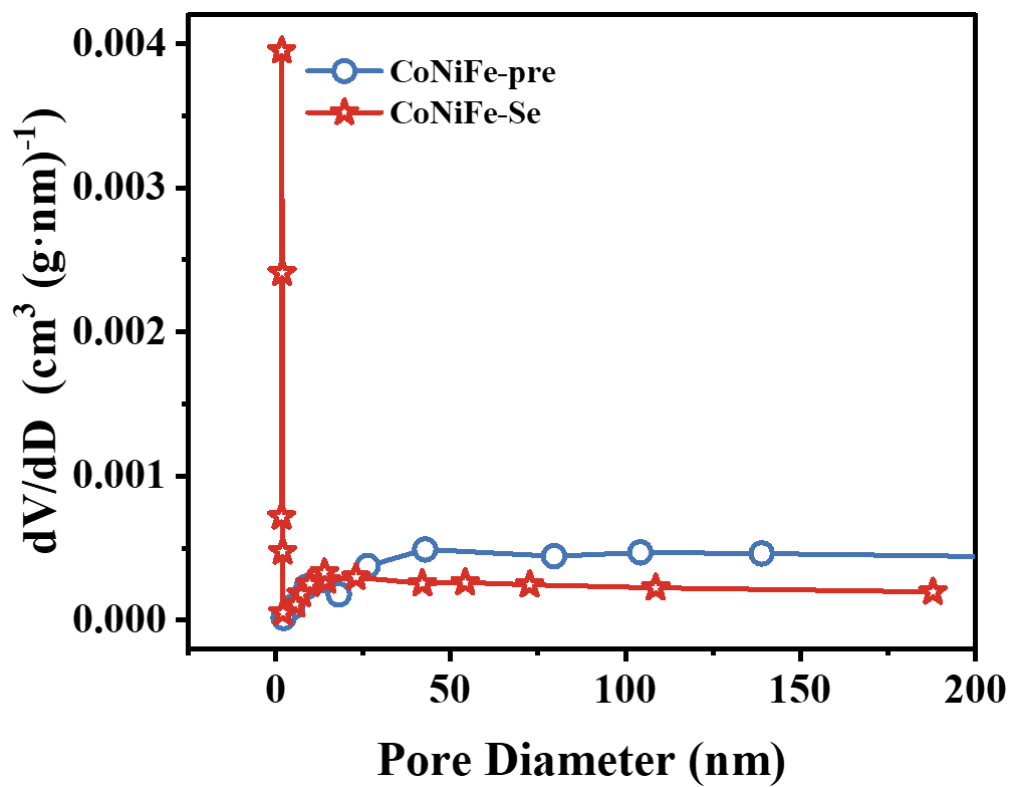
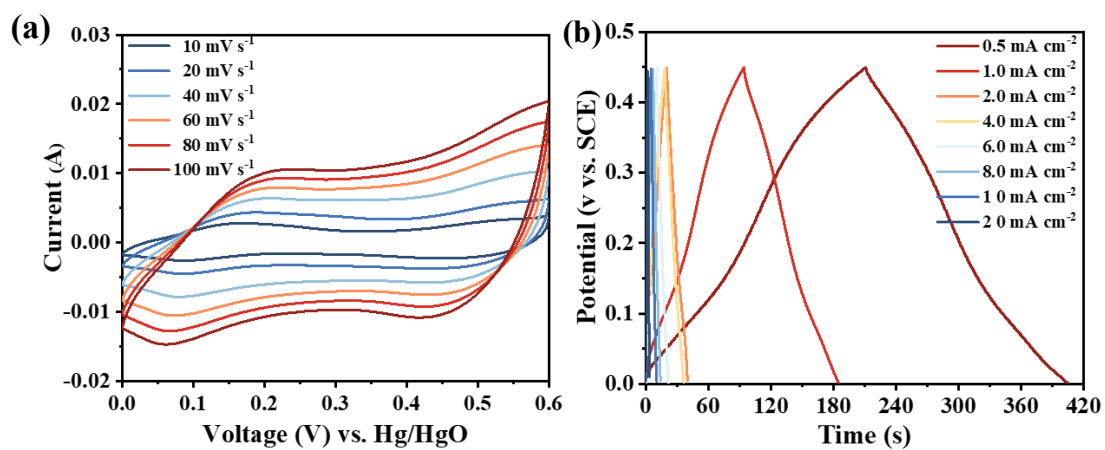
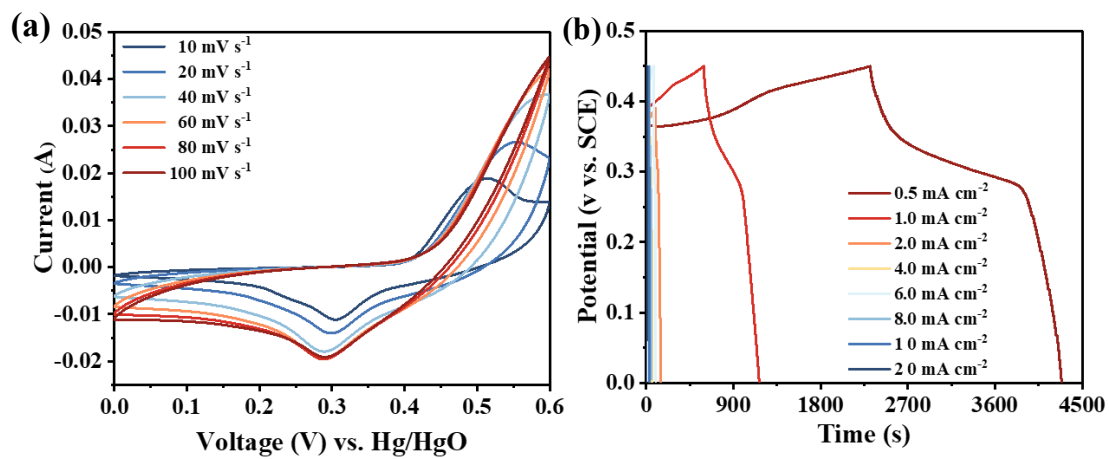


Figure S8. Pore size distribution curves of CoNiFe-pre and CoNiFe-Se.



**Figure S9.** Electrochemical test of Co-Se: (a) CV plots at different scan rates, (b) GCD plots at different current densities.



**Figure S10.** Electrochemical test of Ni-Se: (a) CV plots at different scan rates, (b) GCD plots at different current densities.

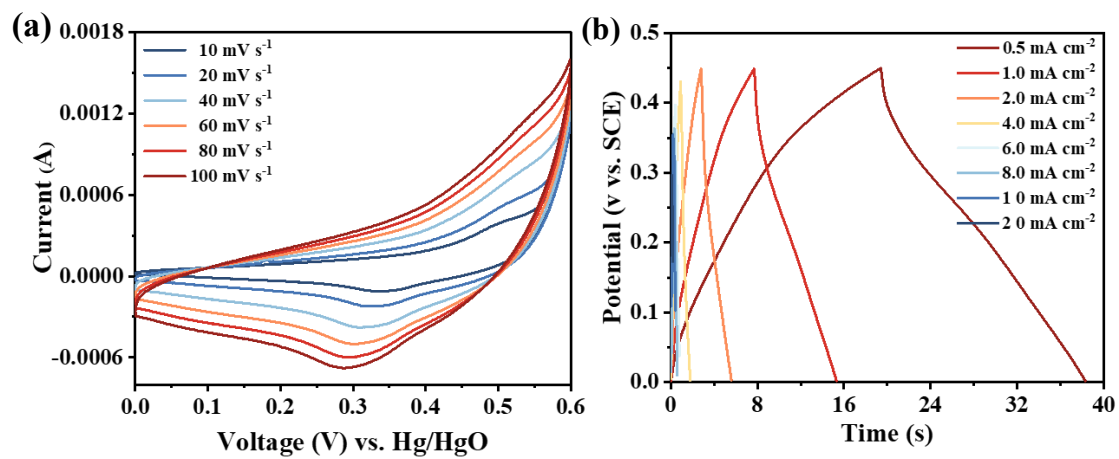


**Figure S11.** Electrochemical test of Fe-Se: (a) CV plots at different scan rates, (b) GCD plots at different current densities.

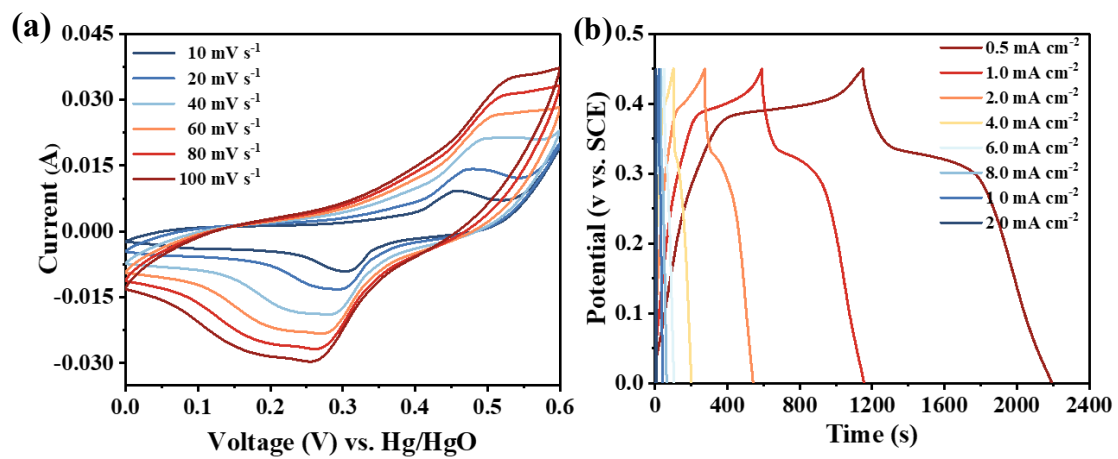


**Figure S12.** Electrochemical test of CoNiFe-pre: (a) CV plots at different scan rates, (b) GCD plots at different current densities.

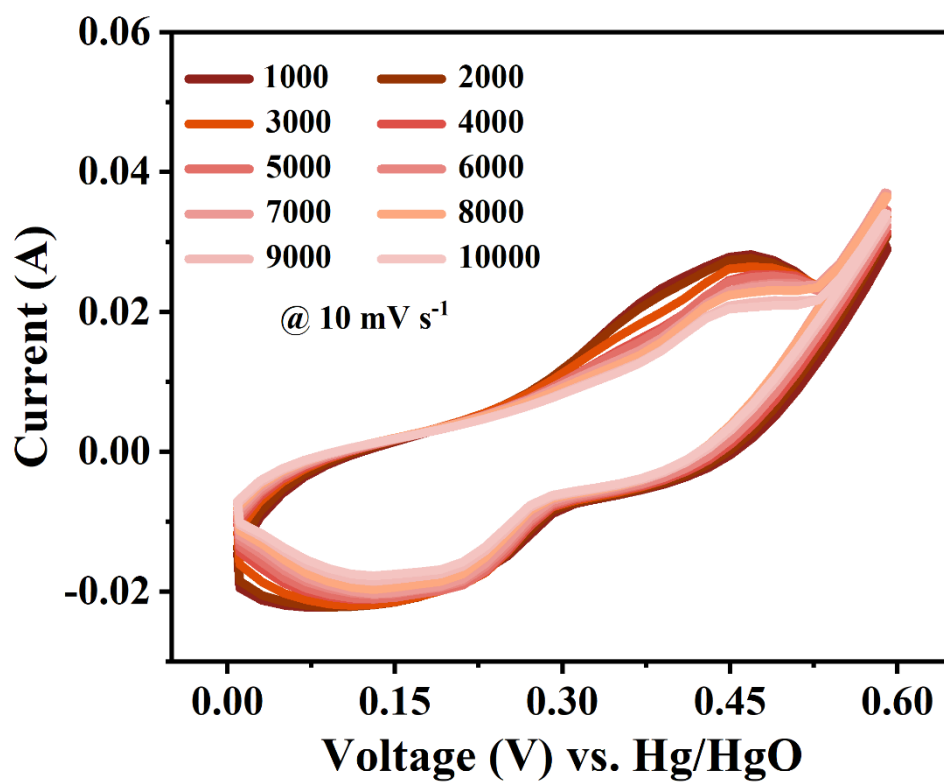
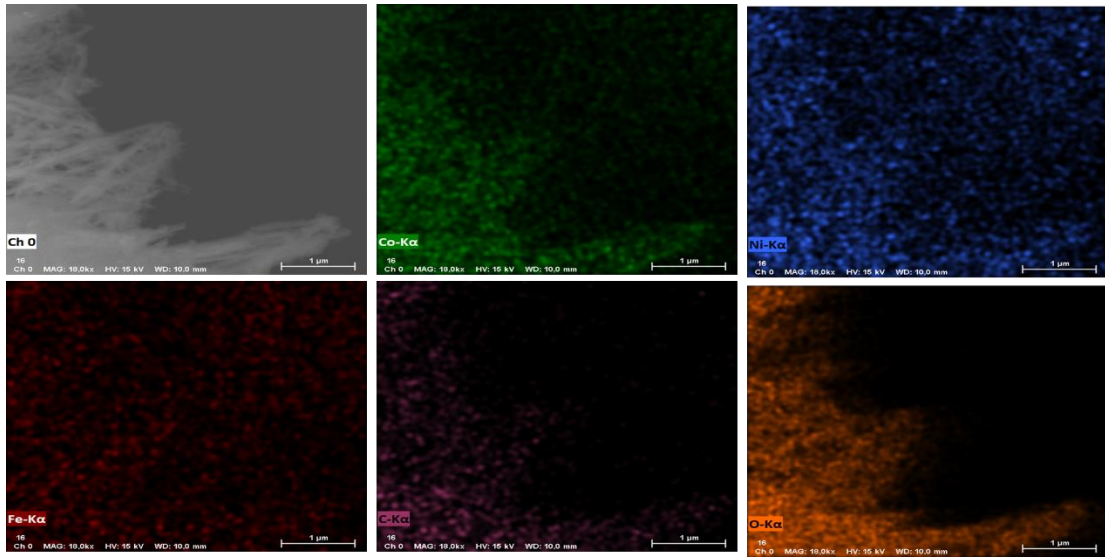
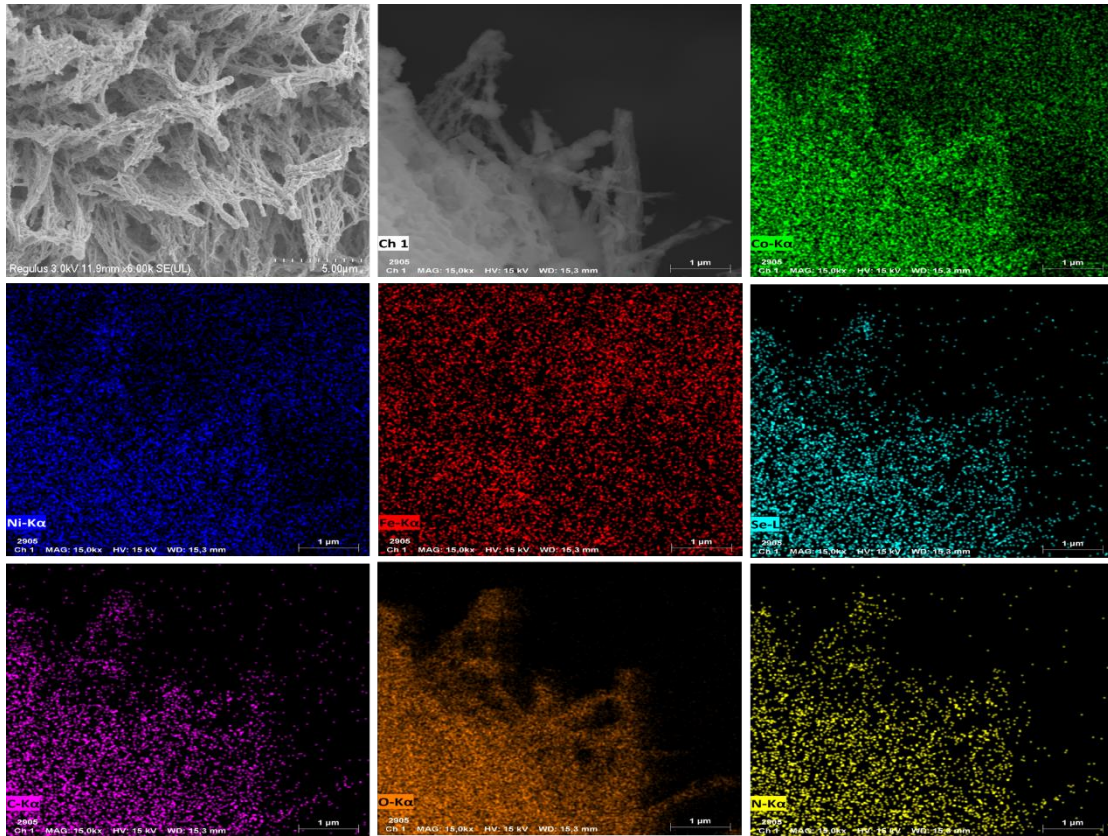


Figure S13. Comparison of CV curves at different cycle numbers for CoNiFe-Se.



**Figure S14.** The SEM and EDS images for CoNiFe-pre after 10000 stability cycles.



**Figure S15.** The SEM and EDS images for CoNiFe-Se after 10000 stability cycles.

After 10,000 cycles, the kebab-like nanostructure remained intact, which also demonstrates the excellent stability of the heterogeneous nanostructure. Moreover, the elements are evenly distributed in the array.

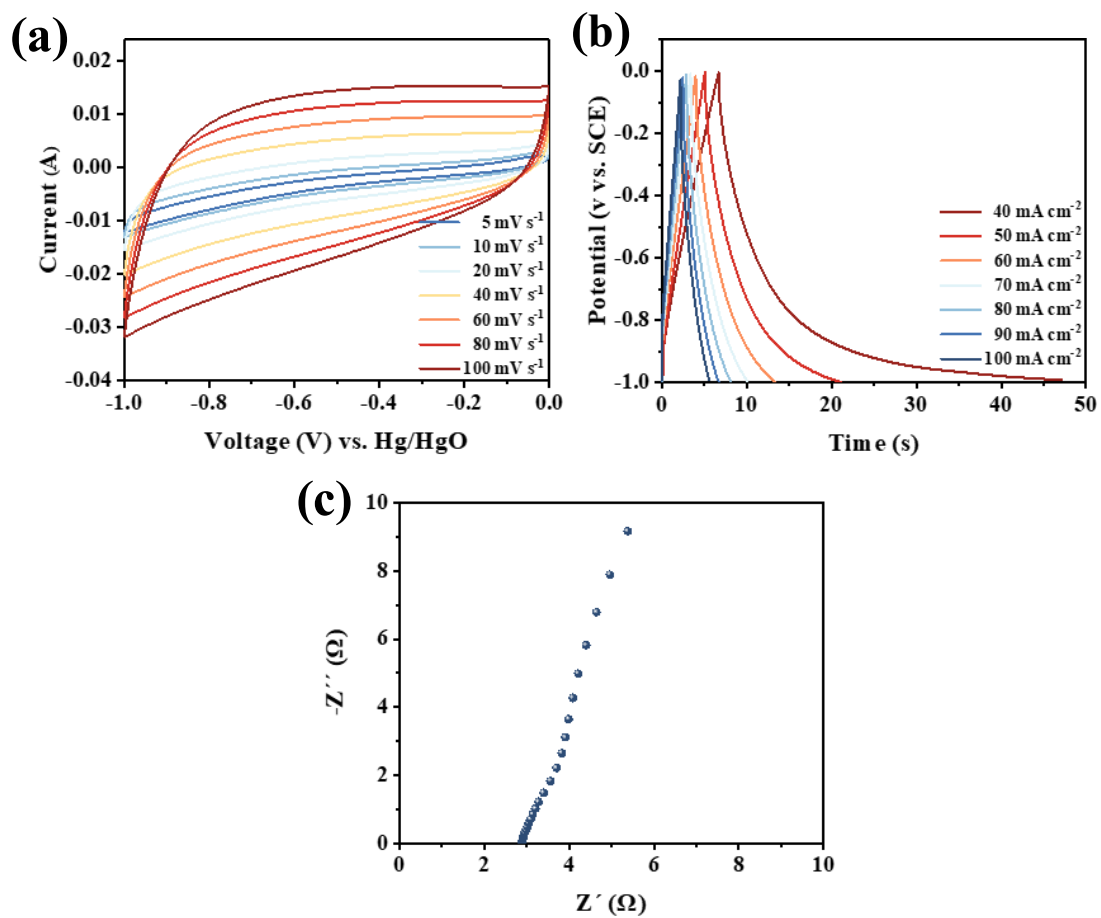


**Figure S16.** Electrochemical testing of AC electrode: (a) CV curves at different scanning rates, (b) GCD curves at different current densities, (c) EIS plot.

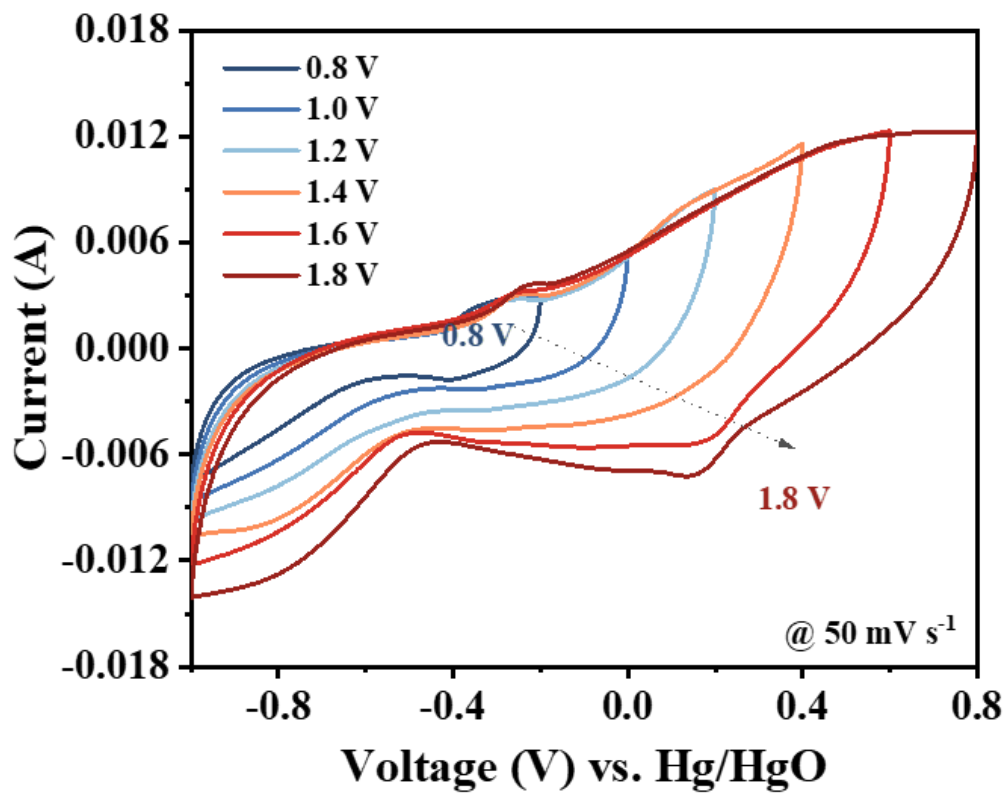


**Figure S17.** Electrochemical testing of ASC device: CV plots of ASC at different potential windows.

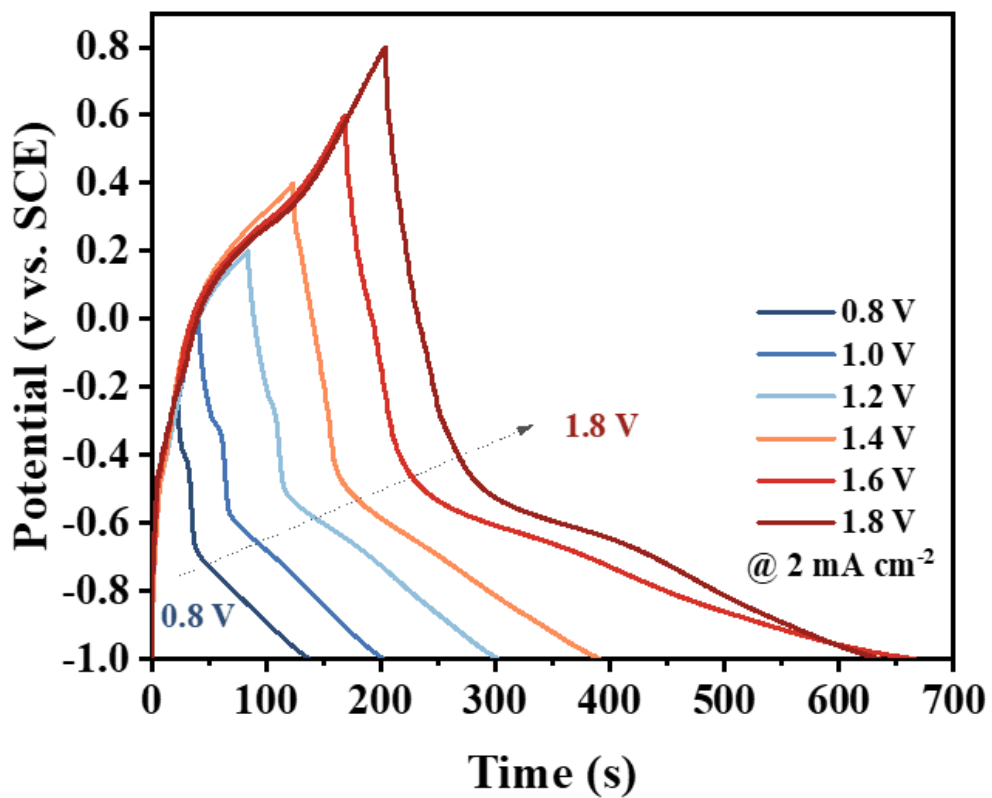
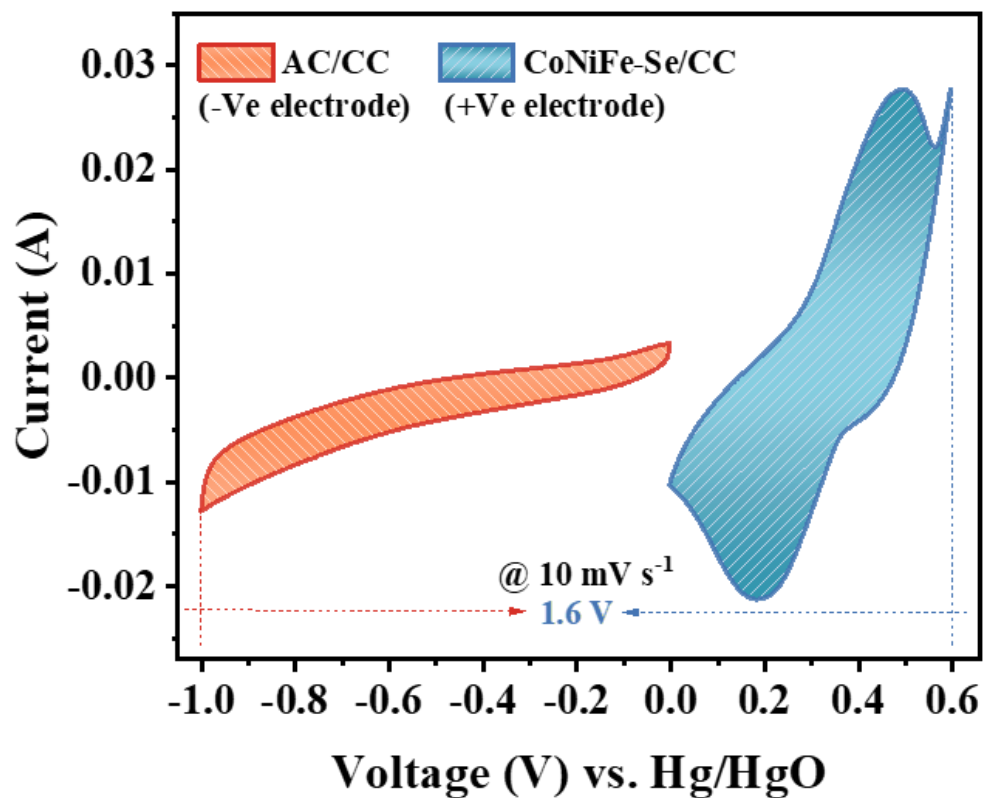


Figure S18. Electrochemical testing of ASC device: GCD plots of ASC at different potential windows.



**Figure S19.** Electrochemical testing of ASC device: CV curves of CoNiFe-Se and AC at a scan rate of 10 mV/s in a three-electrode system.

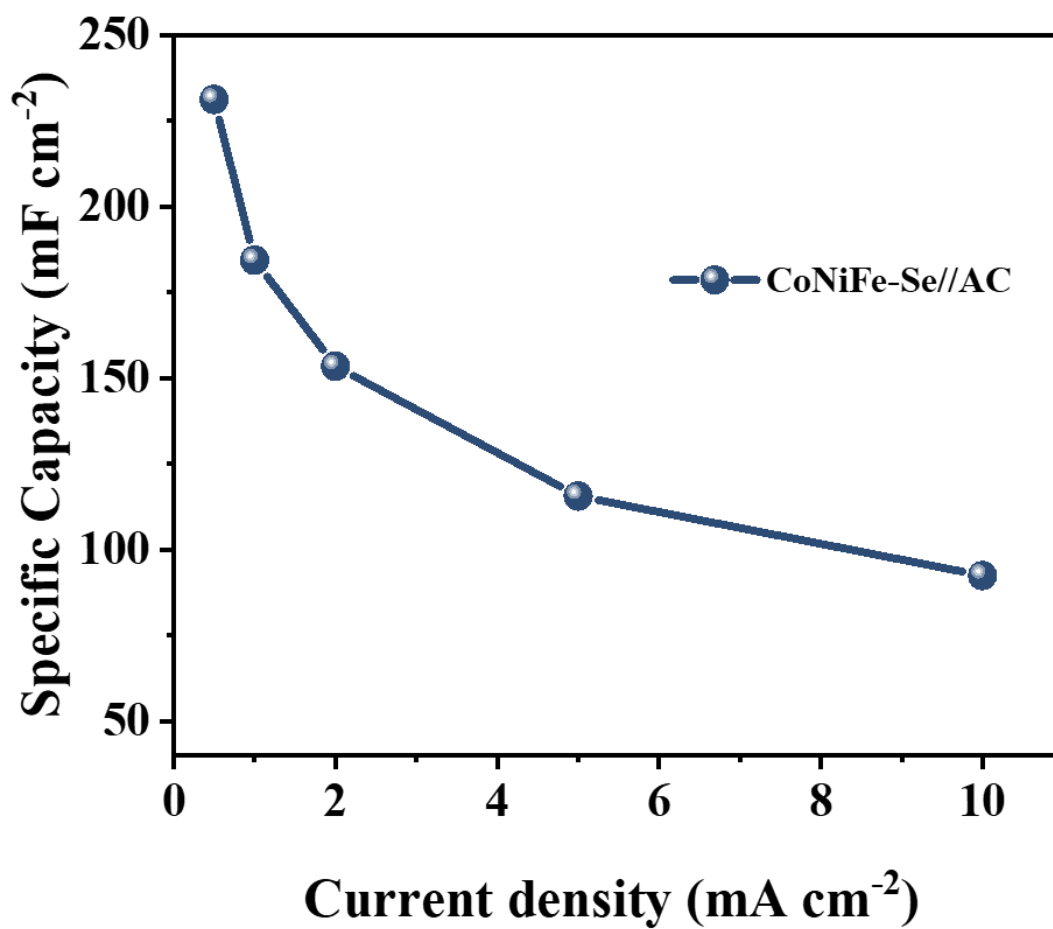
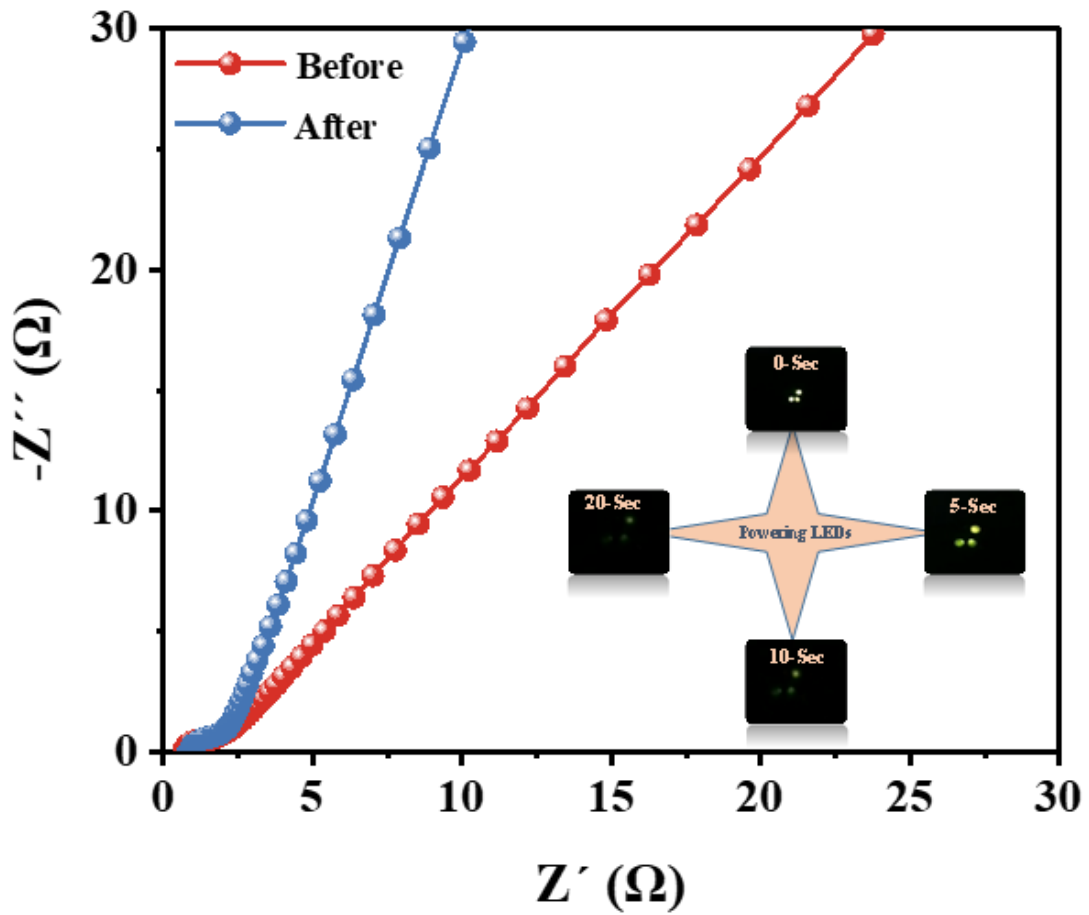


Figure S20. Specific capacitance at different current densities of ASC device.



**Figure S21.** EIS plots of ASC before and after 2000 cycles.

The porous heterostructure of the material provides more space, allowing electrolyte completely permeation and activating the material to achieve steep raising of capacity during the initial cycles. To confirm this, EIS analysis is conducted on the ASC before and after 2000 cycles (Fig. S21). From the Nyquist plots, the smaller radii after 2000 cycles clearly indicates rapid charge transfer due to the excellent porous heterostructure of the material.

**Table S1.** Comparison of transition-metal-based compounds applied to supercapacitors.

Electrode	Electrolyte	specific capacitance	current density	Ref.
Se@(NiCo)Se <sub>2</sub> /CC	3 M KOH	1.73 F cm <sup>-2</sup>	1.8 mA cm <sup>-2</sup>	12
H-Co <sub>0.85</sub> Se NWs	3 M KOH	0.91 F cm <sup>-2</sup>	2.0 mA cm <sup>-2</sup>	13
CoSe/NiSe	6 M KOH	2.90 F cm <sup>-2</sup>	8.0 mA cm <sup>-2</sup>	14
Ni-doped Co <sub>0.85</sub> Se	1 M KOH	1.86 F cm <sup>-2</sup>	20 mA cm <sup>-2</sup>	15
Ni <sub>0.34</sub> Co <sub>0.6</sub> Se <sub>2</sub>	1 M KOH	1.16 F cm <sup>-2</sup>	1.0 mA cm <sup>-2</sup>	16
Cu <sub>2</sub> Se@CuS	6 M KOH	1.9 F cm <sup>-2</sup>	2.5 mA cm <sup>-2</sup>	17
FeCo <sub>2</sub> S <sub>4</sub> /Ni(OH) <sub>2</sub>	6 M KOH	3.07 F cm <sup>-2</sup>	1.2 mA cm <sup>-2</sup>	18
NiCo <sub>2</sub> O <sub>4</sub> -N/GP	3 M KOH	0.19 F cm <sup>-2</sup>	0.8 mA cm <sup>-2</sup>	19
NiCo <sub>2</sub> O <sub>4</sub> microtubes	2 M KOH	1.39 F cm <sup>-2</sup>	2.0 mA cm <sup>-2</sup>	20
Co-Cd-Se	2 M KOH	2.76 F cm <sup>-2</sup>	2.0 mA cm <sup>-2</sup>	21
CCCH@NiCo-LDH@Ag-CuO/Cu	3 M KOH	1.97 F cm <sup>-2</sup>	2.7 mA cm <sup>-2</sup>	22
<b>CoNiFe-Se</b>	<b>6 M KOH</b>	<b>5.0 F cm<sup>-2</sup></b>	<b>1.0 mA cm<sup>-2</sup></b>	<b>This work</b>

**Table S2** The values of  $R_s$  and  $R_{ct}$  for Co-Se, Ni-Se, Fe-Se, CoNiFe-pre and CoNiFe-Se electrodes.

	Co-Se	Ni-Se	Fe-Se	CoNiFe-pre	CoNiFe-Se
$R_s$ ( $\Omega$ )	2.5	3	3.1	3.3	2.2
$R_{ct}$ ( $\Omega$ )	0.162	0.183	0.41	0.189	0.195

**Table S3** Comparison of CoNiFe-pre and CoNiFe-Se electrode in the terms of conductivity.

	Resistivity ( $\Omega \cdot \text{cm}$ )	Conductivity ( $\text{S cm}^{-1}$ )
CoNiFe-pre	1524.390	$6.560 \times 10^{-4}$
CoNiFe-Se	248.416	$4.026 \times 10^{-3}$

**Table S4** The values of  $\tau_0$  for Co-Se, Ni-Se, Fe-Se, CoNiFe-pre and CoNiFe-Se electrodes.

	<b>Co-Se</b>	<b>Ni-Se</b>	<b>Fe-Se</b>	<b>CoNiFe-pre</b>	<b>CoNiFe-Se</b>
$\tau_0$ (s)	0.07	0.02	0.05	0.02	0.01

**Table S5.** Comparison of transition-metal-based materials assembled to SC in the field of supercapacitors.

SC	E ( $\mu\text{Wh cm}^{-2}$ )	P ( $\mu\text{W cm}^{-2}$ )	Ref.
Ni <sub>2</sub> CoS <sub>4</sub> @NiCo <sub>2</sub> O <sub>4</sub> /CFP //N-doped carbon	440	160	23
MWCNTs/CMF	9.8	189.4	24
MWCNTs/CMF	0.42	8.33	25
PNH@NeC-LDH//AC	323	1600	26
NiCo-LDH//AC	80	800	27
NiO// $\alpha$ -Fe <sub>2</sub> O <sub>3</sub>	50	300	28
(NiCo <sub>2</sub> O <sub>4</sub> NG@CF//AC	9.46	500	29
PNC/PEDOT//CMK-3	10	7800	30
Ni-Co DHs/pen ink/nickel //ink/nickel	9.57	492	31
NiO@MnCo-LDH//AC	20	380	32
Co(OH) <sub>2</sub> @Ni-mesh	440	160	33
<b>CoNiFe-Se//AC</b>	<b>221.2</b>	<b>1599</b>	<b>This work</b>

## References

1. Kresse and J. Furthmüller, *Comp Mater Sci.*, 1996, **6**, 15-50.
2. S. Grimme, J. Antony, S. Ehrlich and H. Krieg, *J. Chem. Phys.*, 2010, **132**, 154104.
3. J. Zhao, Y. Wang, Y. Qian, H. Jin, X. Tang, Z. Huang, J. Lou, Q. Zhang, Y. Lei and S. Wang, *Adv. Funct. Mater.*, 2023, **33**, 2210238.
4. W. Kohn and L. J. Sham, *Phys. Rev.*, 1965, **140**, A1133-A1138.
5. J. P. Perdew and Y. Wang, *Phys. Rev. B*, 1992, **45**, 13244-13249.
6. G. Kresse and J. Hafner, *Phys. Rev. B*, 1993, **47**, 558-561.
7. L. Chen, L. Zhou, H. Lu, Y. Zhou, J. Huang, J. Wang, Y. Wang, X. Yuan and Y. Yao, *Chem. Commun.*, 2020, **56**, 9138-9141.
8. J. P. Perdew, K. Burke and M. Ernzerhof, *Phys. Rev. Lett.*, 1996, **77**, 3865-3868.
9. G. Kresse and D. Joubert, *Phys. Rev. B*, 1999, **59**, 1758-1775.
10. G. Kresse and J. Furthmüller, *Phys. Rev. B*, 1996, **54**, 11169-11186.
11. P. E. Blöchl, *Phys. Rev. B*, 1994, **50**, 17953-17979.
12. Y. Guo, X. Hong, Y. Wang, Q. Li, J. Meng, R. Dai, X. Liu, L. He and L. Mai, *Adv. Funct. Mater.*, 2019, **29**, 1809004.
13. Z.-B. Zhai, K.-J. Huang and X. Wu, *Nano Energy*, 2018, **47**, 89-95.
14. F.-X. Ma, L. Yu, C.-Y. Xu and X. W. Lou, *Energy Environ. Sci.*, 2016, **9**, 862-866.
15. F. Liu, L. Zeng, Y. Chen, R. Zhang, R. Yang, J. Pang, L. Ding, H. Liu and W. Zhou, *Nano Energy*, 2019, **61**, 18-26.
16. S. Zhou, Y. Liu, M. Yan, L. Sun, B. Luo, Q. Yang and W. Shi, *Electrochim. Acta*, 2020, **349**, 136337.
17. T. D. Raju, A. Gopalakrishnan and S. Badhulika, *J. Alloys Compd.*, 2020, **845**, 156241.
18. P. Xu, W. Zeng, S. Luo, C. Ling, J. Xiao, A. Zhou, Y. Sun and K. Liao, *Electrochim. Acta*, 2017, **241**, 41-49.
19. C. Xia, Q. Jiang, C. Zhao, P. M. Beaujuge and H. N. Alshareef, *Nano Energy*, 2016, **24**, 78-86.
20. H. Chen, S. Chen, M. Fan, C. Li, D. Chen, G. Tian and K. Shu, *J. Mater. Chem. A*,

- 2015, **3**, 23653-23659.
21. A. Banerjee, S. Bhatnagar, K. K. Upadhyay, P. Yadav and S. Ogale, *ACS Appl. Mater. Interfaces*, 2014, **6**, 18844-18852.
22. Y. Zhao, S. Wang, F. Ye, W. Liu, J. Lian, G. Li, H. Wang, L. Hu and L. Wu, *J. Mater. Chem. A*, 2022, **10**, 16212-16223.
23. V. T. Le, H. Kim, A. Ghosh, J. Kim, J. Chang, Q. A. Vu, D. T. Pham, J.-H. Lee, S.-W. Kim and Y. H. Lee, *ACS Nano*, 2013, **7**, 5940-5947.
24. S. Zhang, B. Yin, Z. Wang and F. Peter, *Chem. Eng. J.*, 2016, **306**, 193-203.
25. B. S. Soram, J. Dai, T. Kshetri, N. H. Kim and J. H. Lee, *Chem. Eng. J.*, 2020, **391**.
26. L. Gao, J. U. Surjadi, K. Cao, H. Zhang, P. Li, S. Xu, C. Jiang, J. Song, D. Sun and Y. Lu, *ACS Appl. Mater. Interfaces*, 2017, **9**, 5409-5418.
27. S. T. Senthilkumar, N. Fu, Y. Liu, Y. Wang, L. Zhou and H. Huang, *Electrochim. Acta*, 2016, **211**, 411-419.
28. L. Gao, R. Fan, R. Xiao, K. Cao, P. Li, W. Wang and Y. Lu, *Appl. Surf. Sci.*, 2019, **475**, 1058-1064.
29. H. Yang, H. Xu, M. Li, L. Zhang, Y. Huang and X. Hu, *ACS Appl. Mater. Interfaces*, 2016, **8**, 1774-1779.
30. X. Wang, X. Li, X. Du, X. Ma, X. Hao, C. Xue, H. Zhu and S. Li, *Electroanal.*, 2017, **29**, 1286-1293.
31. K. Li, M. Liu, S. Li, F. Huang, L. Wang and H. Zhang, *J. Alloys Compd.*, 2020, **817**.
32. X. Dong, Z. Guo, Y. Song, M. Hou, J. Wang, Y. Wang and Y. Xia, *Adv. Funct. Mater.*, 2014, **24**, 3405-3412.
33. L. Cao, G. Tang, J. Mei and H. Liu, *J. Power Sources*, 2017, **359**, 262-269.